1

THIS IS A POST PRINT

A New Method for Estimating of Evapotranspiration and Surface Soil Moisture from Optical and Thermal Infrared Measurements: The Simplified Triangle

Toby N. CARLSON[1], George P. PETROPOULOS[2,3]

[1] *Dept. of Meteorology and Atmospheric Science, Penn State University, University Park, PA 16802, USA*
[2]*School of Mineral & Resources Engineering, Technical University of Crete, Crete, Greece*
[3]*Department of Soil & Water Resources, Institute of Industrial & Forage Crops, Hellenic Agricultural Organization "Demeter", Larissa, Greece*

Correspondence: *Tel: (814) 865-0478 Fax: (814) 865-9429, Email:tnc@psu.edu*

ABSTRACT

Earth Observation (EO) provides a promising approach towards deriving accurate spatiotemporal estimates of key parameters characterizing land surface interactions, such as latent (LE) and sensible (H) heat fluxes as well as soil moisture content. This paper proposes a very simple method to implement, yet reliable to calculate evapotranspiration fraction (EF) and surface moisture availability (M_o) from remotely sensed imagery of Normalized Difference Vegetation Index (NDVI) and surface radiometric temperature (T_{ir}). The method is unique in that it derives all of its information solely from these two images. As such, it does not depend on knowing ancillary surface or atmospheric parameters, nor does it require the use of a land surface model. The procedure for computing spatiotemporal estimates of these important land surface parameters is outlined herein stepwise for practical application by the user. Moreover, as the newly developed scheme is not tied to any particular sensor, it can also be implemented with technologically advanced EO sensors launched recently or planned to be launched such as Landsat 8 and Sentinel 3. The latter offers a number of key advantages in terms of future implementation of the method and wider use for research and practical applications alike.

Keywords: *surface soil moisture, evapotranspiration, triangle method, thermal remote sensing*

1. INTRODUCTION

Currently there is an urgent need for a better understanding of Earth's natural processes and interactions, which is underlined even more in the face of increased pressures from climate change and global food and water security issues (Ireland et al., 2015). In this regard, exact information on the spatiotemporal variation of parameters such as surface soil moisture (SSM) and evapotranspiration (so-called as latent heat flux, LE) is of key significance (Piles et al., 2016). This is due to the influence of these parameters on various physical processes of the Earth system, where they exert a strong control on the Earth's water cycle and ecosystem functioning in general (Shen et al., 2013; Srivastava et al., 2017). Their accurate estimation is also of prime interest for a number of environmental and commercial applications, from sustainable water resource management to evaluating parameterization schemes for weather and climatic models (Liu and Xie, 2013; Bao et al., 2018).

The advent of Earth Observation (EO) technology has provided economically feasible means to derive temporally consistent coverage of those parameters at different spatial scales (Tian et al., 2014). Several EO-based approaches have thus been developed over the past few decades varying from statistical semi-empirical to analytical ones with physical-based algorithms (see reviews by Petropoulos et al., 2015; Petropoulos et al., 2018). These modelling schemes are characterized by varying mechanisms and degrees of complexity, data requirements, basic assumptions, and accuracy. Evidently, there is a specific group of EO-based techniques which aim at deducing surface fluxes of LE, H and/or SSM at a variety of spatial and temporal scales based on the synergy of satellite data from optical (visible and infrared - VNIR) and thermal infrared (TIR) radiometers. Those methods, commonly termed in the literature as T_s/VI methods, are based on the physical relationships that exist when a satellite-derived land surface temperature (T_s) is plotted against a spectral vegetation index (VI).

It has been demonstrated that the derivation of spatially distributed estimates of energy fluxes and SSM using the T_s/VI 'triangular' scatterplot is feasible without the use of a boundary layer model. Yet, more sophisticated approaches tend to involve the use of a land biosphere model, specifically of a Soil Vegetation Atmosphere Transfer (SVAT) model, via a technique commonly termed as the "triangle". Various validation studies have demonstrated its ability to provide estimates of both surface heat fluxes and SSM with accuracies in the order of 40 to 70 Wm^{-2} and within 5 % vol vol^{-1} for SSM over homogenous areas (Gilles et al., 1997; Owen et al. 1998; Jiang et al., 2001; Carlson, 2007; Tang et al., 2010; 2013). The significant prospect of the Ts/VI scatterplot methods and of the "triangle" in particular, is documented by the fact that variants of this technique are considered at present in operational products development of energy fluxes and/or SMC on a global scale (Chauhan et al., 2003; ESA STSE, 2012). Also, a variant of the "triangle" it already deployed today over Spain to operationally deliver SSM maps at 1 km spatial resolution from ESA's own SMOS satellite (Piles et al., 2011; 2014). Thus, from the above it becomes evident that research focusing on the "triangle" implementation is undoubtedly of key interest, particularly so given the fact that variants of this method are being explored today for operational implementation.

In this context, the present study aims at introducing the "simplified triangle" method, which represents an extension of the so-called 'triangle" method. This new method allows one to estimate surface evapotranspiration fraction (EF) and surface soil moisture availability (M_o) over an area using just a few simple calculations in conjunction with satellite or aircraft images made at optical wavelengths and in the thermal infrared. Two parameters are derived from the simplified triangle method, a surface wetness, represented by the parameter M_o, and the evapotranspiration fraction EF. The former is defined as the ratio of soil surface evaporation ETs to the potential evapotranspiration (ET_s/ET_{pot}), but is also loosely equated with the ratio of soil water content to that at field capacity. EF is defined as the ratio of evapotranspiration to net radiation (R_n). The simplified triangle method has a great advantage over other methods belonging to this same group of models in that it does not require a land surface model or ancillary surface or atmospheric data for its execution and, as such, it is practical and easy to apply. It should be noted that recently, a pair of similar models (referred to as trapezoid models has been published (Sadeghi et al., 2017; Babaeian et al., 2018). As in the simplified triangle model, these two models also require no ancillary data, but use the short wave solar radiation both in addition to and as an alternate to surface radiometric temperature, the former aimed for use with satellites for which no thermal sensors exist.

2. INPUT PARAMETERS

To implement the "simplified triangle", two image fields required, as obtained from satellite (or aircraft) measurements: the surface radiometric temperature (T_{ir}) and the normalized difference vegetation index (NDVI). The latter is derived from a pair of radiances measured at two wavelengths in the solar spectrum, one in the visible and one in the near infrared. NDVI is defined as:

$$NDVI = (R_{NIR} - R_{RED})/(R_{NIR} - R_{RED}) \quad (1)$$

Here, R_{NIR} and R_{RED} are the reflectance values measured, respectively, in the near infrared (e.g. a wavelength just above 0.7 microns, as from channel 4 of Landsat 8 sensor) and in the visible (e.g. a wavelength near 0.65 microns, as from channel 3 of Landsat 8 sensor). Calculation of the fractional vegetation cover from NDVI is described below.

As defined, M_o applies only to the top few millimeters of the bare soil surface. Similarly, the bare soil surface radiometric temperature (T_s) applies to the bare soil surface. T_{ir}, of course, pertains to a mixture of the bare soil surface (T_s) and the vegetation canopy temperature T_{veg}.

3. IMAGE SELECTION

In order to minimize measurement errors, the two images, those of T_{ir} and NDVI, must represent a reasonably uniform terrain height (not varying by more than about 10%) and should not contain a large fraction of standing water or cloud. Although different vegetation types may be present in the image without great loss of accuracy, highly inhomogeneous vegetation such as a forest situated aside a field of corn or grass might introduce some error (including edge effects) in the derived surface parameters (Carlson & Sanchez-Azofeifa, 1999). If the image contains some standing water or cloud, these effects first must be removed, a process that can be done by a judicial analysis of the reflectance pattern.

Estimate of the salient features discussed in Section 6 depends on having at least some bare soil and fully vegetated pixels in the image. It seems quite likely that bare soil and vegetation coexist in at least a few pixels in images taken over a larger enough area. Fractional vegetation cover (F_r; defined below) for each pixel is calculated and the end point parameters discussed in the next section are then able to be determined.

4. METHOD DEMONSTRATION

Now, consider the two images made over an area, one for T_{ir} and the other for NDVI. The first step is to identify some pixels representative of dense vegetation (full vegetation cover) and some of dry, bare soil, as illustrated in the example shown in Figure 1. In these two images, the pixels with highest and lowest values of radiometric surface temprature are indicated in the upper left image and those pixels with the highest and lowest values of NDVI are indicated in the lower right image.

Corresponding surface pixels selected in these two images represent the hottest and least vegetated pixels (over dry, bare soil) such as found over a paved urban area (parking lot, city center, etc.). Two other pairs of arrows denote densely vegetated terrain, such as found in the countryside. Highest values of surface temperature (red areas in the temperature image) likely represent pixels with zero surface soil moisture, while those over dense vegetation correspond to a full vegetation cover and a source of potential transpiration (the dense green areas in Figure 1).

If pixels can be found that lie over patches of dense vegetation that is not wilted, they define the full vegeation cover condition where the fractional vegetation cover (Fr) equals 1.0 There, T_{ir} is equal to T_{min}, and NDVI is defined as $NDVI_s$ (the arrow pointing to a green patch in the NDVI image of Figure 1). Similarly, the maximum temperatures (the arrow pointing to a red patch in the temperature image and a white patch in the NDVI image of Figure 1) define the bare soil condition (F_r=0) and the maximum temperature Tmax, where the bare soil NDVI is defined as $NDVI_o$.

[FIGURE 1 GOES HERE]

Having defined these points on the image, the next step is to calculate fractional vegetation cover and Surface Temperature from NDVI. A useful relationship (Gilles et al., 1997) is:

$$F_r = ((NDVI - NDVI_o) / (NDVI_s - NDVI_o))^2 \qquad (2)$$

Similarly, we introduce the very important concept of a *scaled* infrared surface temperature T* defined as

$$T^* = (T_{ir} - T_{min}) / (T_{max} - T_{min}) \qquad (3)$$

Both the scaled T_{ir} (now called T^*) and the fractional vegetation cover F_r are thus constrained to vary between 0 and 1.0. T^* is sometimes referred to as the 'temperature-dryness index' (Sandholt et al., 2002).

As shown by Carlson and Ripley (1997), F_r is highly insensitive to atmospheric attenuation effects on NDVI, so that the method requires no correction for NDVI. Although it has not been conclusively demonstrated, it is quite likely that the scaled temperature T* is less sensitive to atmospheric attenuation than T_{ir} itself because scaling should tend to at least partially cancel the atmospheric correction. This is not a settled issue and the user is free to introduce corrections to T_{ir} for atmospheric attenuation. Our assumption for not correcting T_{ir} for atmospheric attenuation rests partly on analogy with NDVI, but also on the fact that the values of M_o and EF are constrained to vary within the triangle between the values of zero and one. Neglect of atmospheric attenuation greatly reduces image processing time without necessarily engendering serious error. Scaling will also remove errors due to sensor calibration.

As an example of calculating T^*, consider Figure 1. Here, maximum and minimum NDVI and T_{ir} for the case represented, chosen subjectively by eye, are NDVIs = 0.82, NDVIo = 0.18, T_{max} = 296.3K (23.0 ° C), T_{min} = 287.5K (14.2 ° C), so that. T* varies over a range of 8.8 °C. A value of T*=0.5 corresponds to T_{ir} = 18.6. Similarly, the range of NDVI is 0.64, so that a value of NDVI = 0.50 yields a value of F_r (Equation 2) of 0.25.

5. TRIANGLE CONSTRUCTION

The triangle is best viewed by plotting pixels for T* and Fr on a two dimensional space as in Figure 2. The latter represents a raw image uncorrected for standing water and cloud. It exhibits considerable scatter due to standing water and cloud near the bottom and especially on the left.

One can filter these effects by realizing that clouds tend to be cold and highly reflective but yield low values of NDVI while standing water tends to be cold but with very low reflectance and very low values of NDVI. Once, cloud and standing water pixels have been removed the resulting configuration is a better defined triangular or trapezoidal feature (Figure 3). Although the shape of the triangle tends to degrade as the resolution of the radiometer decreases it appears even at 1 km resolution, such as for AVHRR images (Figure 2).

[FIGURE 2 GOES HERE]

6. ESSENTIAL FEATURES OF THE TRIANGLE

A striking feature of this kind of pattern shown in Figures 2 and 3 is the very sharp edge on the warm side of the pixel envelope, which we define as the *warm edge*. It could just as well be called the dry edge as it represents the limit of *surface* soil dryness which we assume also corresponds to a line along which M_o=0. The base of the triangle, which is sometimes referred to as the *soil line*, corresponds to F_r=0. A corresponding *cold edge*, defining the isopleth M_o=1.0, is also shown, though this line is sometimes blurred by scatter. Finally, the top (*vertex*) of the triangle corresponds to full vegetation cover, F_r=1.0, although at that point the soil, being largely obscured by vegetation, M_o values are not resolvable.

Figure 3 shows the warm and cold edges, the soil line and the triangle's vertex. Now, let us examine these salient features of the triangle in more detail.

warm edge: The characteristic sharply defined warm side of the triangle can, provided that the feature is a right triangle, be ruled by eye from the lower right-hand vertex (F_r=0 ($NDVI_o$), T_{max}) to the upper vertex (F_r=1.0; $NDVI_s$). If the vertex is well-defined, this point is found at $NDVI_s$, T_{min}. Some researchers (Tang et al. 2010) divide up slices of F_r between the cold and warm edges into segments of T^*, and define the warm edge as the point where the pixel density in these segments, in moving from cold to warm, decreases to some small number or where, say, 99% of the pixels have been sampled in that slice, at which point the value of T^* is recorded. Once these points have been determined for a series of points at various values of F_r, a straight-line represents the best fit of the warm edge to these end points at different values of F_r.

For a triangle with a well-defined upper vertex, the slope of the line between T^* of zero and one is always.

$$T^*(\text{warm edge}) = 1-F_r \tag{4a}$$

In the more general case, a regression line (Equation 4b) is fit to the warm edge using the unscaled T_{ir} (e.g., Sandholt et al., 2002; Tang et al., 2010).

$$T_{ir}\ (\text{warm edge}) = \alpha+\beta \times (\text{NDVI}) \tag{4b}$$

where constants α and β define the best fit linear regression of NDVI versus T_{ir} along the warm edge. Note that Tir must always be equal to or less than T_{ir} along the warm edge.

The triangular scatterplots in shown in Figure 4 are among many similar ones from this same data set (Silva-Fuzzo & Rocha, 2016). Here, the slanting red lines (determined visually) make reasonable (if not precise) fits to the warm edge of the pixel envelope.

Some researchers contend that the scatter of points beyond the warm edge represents water stressed vegetation, but this has not been proved and can also be due to sloping terrain.

[FIGURE 3GOES HERE]

cold edge: This feature, which represents the limit of wetness, tends to be less well defined than the warm edge. Pixels usually form a less sharp border than for the slanting warm edge, but the border constituting the cold edge tends to be vertically orientated along a straight line drawn between the point (F_r=1.0, T_{min}) and (F_r=0; T_{min}), as discussed by Jiang et al. (2001, Sandholt et al. (2002) and Kasim (2015). Figure 4 (and many others not shown here) attests to the verticality of the cold edge. While some triangles sometimes tilt toward the left, as can be seen in Figure 3, we think that the absence of pixels near the lower left part of the triangle in these cases is due to the rarity of truly wet, bare soil surfaces.

Soil line: The bare soil line, ($NDVI_o$) can also be determined by eye or by a statistical test as just mentioned with regard to the warm edge. Figure 4 shows triangles with fairly well-defined bases, although one might contend with the exact locations of the soil line in Figure 3 and the warm edges in Figure 4.

[FIGURE 4 GOES HERE]

Triangle vertex: Some triangles appear with rounded or flattened tops, more closely resembling trapezoids. This could be due to various factors. Some researchers believe the variation of T^* at the point where F_r=1.0 is due to a real variation in leaf temperature due to water stress (Petropoulos et al., 2009). An alternate possibility is that the highest values of NDVI do not represent a truly 100% vegetation cover.

Simulations with a Soil-Vegetation-Atmosphere-Transfer (SVAT) model, the model being described in Petropoulos et al. (2009), suggest that a flattened top can appear in a full vegetation cover not under stress if the leaf area index (LAI) is not very large, say close to 3, in which case some holes exist in the vegetation canopy. If so, sharp vertices in a triangle may signify that the LAI is very much larger than 3.

7 SOLUTIONS FOR Mo AND EF

The geometry presented here presumes that M_o and EF vary linearly across the pixel domain. Thus, from Figure 5 we see that M_o is just the ratio of the segments (a/d) (Petropoulos et al., 2009). Mathematically, geometry requires that

$$Mo = (1-T^{*}_{pixel}) / T^{*}\ (\text{warm edge}) \tag{5}$$

where T^{*}_{pixel} must always be less than or equal to that along the warm edge. Thus, if the pixel envelope is a triangle:

$$M_o = (1-T^{*}_{pixel})/(1-F_r) \tag{6}$$

$$EF = EF_s \times (1-Fr) + EF_{veg} \times F_r \tag{7}$$

Equation 7, F_r is the fractional vegetation cover, EF is weighted by the fractional vegetation cover, where the soil component EF_s (the ratio of soil evaporation to net radiation) is equal to M_o and EF_{veg} = 1.0 for the vegetative component. This equation simplifies to the very simple expression

$$EF = M_o \times (1-F_r) + F_r \tag{8}$$

Note that one can substitute Equation 4b in Equation 5 if the triangle has a flat top and the warm edge is determined by a regression line.

[FIGURE 5 GOES HERE]

Figure 6 is a graphical representation for the solution to Equations 5-8, illustrating that the isopleths of M_o and EF are sloping straight lines within the triangle. As such, Figure 6 constitutes a universal solution for all triangles. If triangles are plotted on the same scale in which vertices vary from zero to one, they are all congruent.

Imagine a series of such triangles created over a period of days and stacked vertically in chronological order, the triangle representing the earliest image on the bottom and later ones above. The vertical axis is now that of time. Such a representation allows the user to chart the temporal movement of M_o and EF at specific land surface points, so the progress of surface drying can be monitored (Carlson & Arthur, 2000; Owen et al., 1998; Carlson & Sanchez-Azofeifa, 1999). An example of this type of time variation of a pixel is illustrated schematically by the arrow in Figure 6, showing a progressive drying of the surface point as the point moves downward and to the right with time.

Cases where the scatterplot more closely resembles a trapezoid than a triangle with a sharp upper vertex may occur because pixels chosen to represent a dense vegetation canopy may actually not be representative of a full canopy in which no direct solar radiation is reaching the soil surface. A better choice of $NDVI_s$ might then by at the apex of a virtual triangle created using the regression line (Equation 4b) to extrapolate the warm edge to the point where $T^*=0$ (along the cold edge). Similarly, where the line representing the warm edge does not fit snugly against the pixel envelope, a judicious revision of the initial choices of T_{max} or $NDVI_s$ can be achieved using the regression Equation 4b to extrapolate T_{ir} to better choices of these end points.

[FIGURE 6 GOES HERE]

8. VALIDATION OF METHOD

Figure 7 shows isopleths of M_o and EF derived from a full soil /vegetation/ atmosphere/transfer (SVAT) model for a triangular pixel distribution over crops in Costa Rica (Carlson & Sanchez-Azofeifa, 1999). Note that isopleths of M_o are nearly straight lines that slope upward to the left, very similar to those for Mo in the universal triangle, shown in Figure 6.

Isopleths of EF, however, though deviating from straight lines in the SVAT model representation (Figure 7) still agree reasonably closely with those from the universal triangle (Figure 6), the largest differences occurring near the lower left side of the triangles. In comparing these two figures, differences in Mo and EF are generally less than 0.15. Recent simulations (Kasim, 2019; private communication) show no significant differences for M_o estimated from the simplified triangle method and that derived from a full SVAT model (described in Petropoulos et al., 2009). Yet, the latter remains to be investigated in detail in the future. The methodology appears to have worked well when applied to a study of soybean productivity in Brazil in which EF was used to predict crop yield (Silva-Fuzzo & Rocha, 2016). Certainly, more validation studies are needed to lend further credence to the STM.

[FIGURE 7 GOES HERE]

9. SUMMARY

The simplified triangle method allows one to estimate the surface soil moisture availability and the evapotranspiration fraction without the aid of a land surface (e.g., SVAT) model and without the need for ancillary surface and atmospheric information. As such, the method is not only fast and easy to apply, but it is especially useful in regions with little ancillary atmospheric or surface data. Those who are unfamiliar with mathematical representations of land surface and atmospheric parameters or who wish only a quick and easy method to estimate the surface soil wetness and evapotranspiration might find this method more appealing than one that requires more complexity. Moreover, the ‘universal triangle’ affords a graphic representation of land surface changes with time.

Although more investigation is necessary in order to fully assess the accuracy of the simplified triangle method, in comparison with estimates made with the aid of more complex land surface models, preliminary indications based on papers in print or under review (cited above) suggest that the results from both methods would be very similar. Two papers by Silava-Fuzzo and Silva-Fuzzo et al, cited in this paper, show that the values of EF generated from the simplified triangle method produced good estimates of soybean yields over Brazil.

Two aspects of this model appear to trouble some of its users. One is the idea of scaling and the other pertains to the extraction of the relevant end values for NDVI and T_{ir}. We hope that this paper will help clarify the scaling process. To date, however, no satisfactory method has been demonstrated that allows the user to extract these parameters objectively. Instead, one is forced to do this manually, with the interplay of hand and eye, while noting the values designated by the cursor at the appropriate bare soil and dense vegetation locations. A highly practical advance in this method, therefore, would be to develop an operational system in which the triangles and their relevant parameters are determined operationally with intelligent software using only NDVI and T_{ir} images.

We suggest that, once the method is satisfactorily validated, the next step in its development would be to implement it operationally. The use of the “triangle” exploiting EO data from with these new satellite sensors remains to be seen.

ACKNOWLEDGEMENTS

Dr Petropoulos contribution has been supported by the FP7- People project ENViSIoN-EO (project reference number 752094) and the author is grateful to the funding body for the financial support provided. Sincere thanks also go to Erin Grebb helped with the figures’ improvement in the manuscript. Authors wish to also thank the anonymous reviewers and the handling editor for their useful comments, which resulted to improving the initially submitted manuscript.

REFERENCES

ARTHUR-HARTRANFT, S.; CARLSON, T. N.; CLARKE, K., 2003. Satellite and ground-based microclimate and hydrologic analyses coupled with a regional urban growth model. *Remote Sensing of Environment,* **86**, 385-400.

BABAERIAN, E., SADEGHI, M., FRANZ , T. E., JONES, S., TULLEER, M., 2018. Mapping soil moisture with the Optical TRApezoid Model (OPTRAM) based on long-term ODIS observations Ebrahim. *Remote Sensing of Environment*, **211**, 425-440.

BAO, Y., L. LIN, S. WU, K.A.K. DENG & G.P. PETROPOULOS, 2018. Surface Soil Moisture Retrievals Over Partially Vegetated Areas From the Synergy of Sentinel-1 & Landsat 8 Data Using a Modified Water-Cloud Model. *International Journal of*

Applied Earth Observation & Geoinformation, **72**, 76-85, /doi.org/10.1016/j.jag.2018.05.026.

CARLSON, T. N. 2007. An overview of the triangle method for estimating surface evapotranspiration and soil moisture from satellite imagery. *Sensors MDPI,* **7**, 1612-1629.

CARLSON, T. N., 2013. Triangle models and misconceptions. *Int. J. of Remote Sensing Applications.* **3**, 155-158.

CARLSON, T. N.; ARTHUR, S. T., 2000. The impact of land use-land cover changes due to urbanization on surface microclimate and hydrology: a satellite perspective. *Global and Planetary Change*, **25**, 40-65.

CARLSON, T. N.; RIPLEY, D. A.,1997. On the relation relationship between NDVI, fractional vegetation cover and leaf area index. *Remote Sensing of Environment,* **62**, 241-252.

CARLSON, T. N.; SANCHEZ-AZOFEIFA, G. A., 1999. Satellite remote Sensing of land use changes in and around San Jose', Costa Rica. *Remote Sensing of Environment*, **70**, 247-256.

CHAUHAN, N. S., MILLER, S., ARDANUY, P., 2003. Spaceborne soil moisture estimation at high resolution: a microwave-optical/IR synergistic approach. *International Journal of Remote Sensing*, **22**, 4599-46.

EUROPEAN SPACE AGENCY: SUPPORT TO SCIENCE ELEMENT, 2012. A pathfinder for innovation in Earth Observation, 41 pp., available at: http://due.esrin.esa.int/stse/files/document/STSE_ report_121016.pdf (last access: 10 July 2013), ESA, 2012.

GILLIES, R. R.; CARLSON, T. N; CUI, J.;KUSTAS, W. P.; HUMES, K. S.,1997. A verification of the 'triangle' method for obtaining surface soil water content and energy fluxes from remote measurements of the Normalized Difference Vegetation Index (NDVI) and surface radiometric temperature. *International Journal of Remote Sensing*, **18**, 3145-3166.

IRELAND, G., PETROPOULOS, G. P., CARLSON, T. N., PURDY, S., 2015. Addressing the ability of a land biosphere model to predict key biophysical vegetation characterisation parameters with Global Sensitivity Analysis. *Environmental Modelling & Software*, 65, 94-107.

JIANG, L.; ISLAM, S., 2001. Estimation of surface evaporation map over southern Great Plains using remote sensing data. *Water Res. Research.* **37**, 329-340.

KASIM, A. A., 2015. Derivation of surface soil water content using a simplified geometric method in Allahabad District, Uttar Pradesh, India. *International Journal of Scientific Research.* **6**, 1631-1637.

LIU, J. G., XIE, Z. H., 2013. Improving simulation of soil moisture in China using a multiple meteorological forcing ensemble approach. *Hydrology and Earth System Sciences Discussions*, **10**(3): 3467-3500.

OWEN, T. W.; CARLSON, T. N.; GILLIES, R. R., 1998. An assessment of satellite remotely-sensed land cover parameters in quantitatively describing the climatic effect of urbanization. *International Journal of Remote Sensing*, **9**, 1663-1681.

PETROPOULOS, G.; CARLSON, T. N.; WOOSTER, M.; S. ISLAM, S., 2009. A review of Ts/VI remote sensing based methods for the retrieval of land surface energy fluxes and soil surface moisture. *Progress in Physical Geography*. **33**, 224-250.

PETROPOULOS, G.P., IRELAND, G. & B. BARRETT, 2015. Surface Soil Moisture Retrievals from Remote Sensing: Evolution, Current Status, Products & Future Trends. *Physics and Chemistry of the Earth*. DOI: 10.1016/j.pce.2015.02.009.

PETROPOULOS, G.P., P.K. SRIVASTAVA, K.P. FEREDINOS & D. HRISTOPOULOS, 2018. Evaluating the capabilities of optical/TIR imagine sensing systems for quantifying soil water content. *Geocarto International*, DOI 10.1080/10106049.2018.1520926

PILES, M, A. CAMPS, M. VALL-LLOSSERA, A. MONERRIS, M. TALONE, 2011. Downscaling SMOS-derived soil moisture using MODIS visible/infrared data. *IEEE Transactions on Geoscience and Remote Sensing*. **49**, pp. 3156 – 3166, doi: 10.1109/TGRS.2011.2120615.

PILES, M, M VALL-LLOSSERA, A. CAMPS, N. SÁNCHEZ, J. MARTÍNEZ-FERNÁNDEZ, J. MARTÍNEZ, V. GONZÁLEZ-GAMBAU, 2013. On the synergy of SMOS and Terra/Aqua MODIS: high resolution soil moisture maps in near real-time, *Proc. IEEE International Geoscience and Remote Sensing Symposium*, pp. 3423-26. doi: 10.1109/IGARSS.2013.6723564.

PILES, M., G.P. PETROPOULOS, N. SANCHEZ, A. GONZÁLEZ-ZAMORA & G. IRELAND, 2016. Towards Improved Spatio-Temporal Resolution Soil Moisture Retrievals From the Synergy of SMOS & MSG SEVIRI Spaceborne Observations. *Remote Sensing of Environment,* **180**, pp:403-471, DOI 10.1016/j.rse.2016.02.048

PILES, M., SÁNCHEZ, N., VALL-LLOSSERA, M., CAMPS, A., MARTÍNEZ-FERNÁNDEZ, J., MARTÍNEZ, J., & GONZÁLEZ-GAMBAU, V., 2014. A dowscaling approach for SMOS land observations: long-term evaluation of high resolution soil moisture maps over the Iberian Peninsula. *IEEE Journal of Selected Topics in Applied Earth Observations and Remote Sensing*, **7**, 3845-3857.

PRICE, J. C., 1990. Using spatial context in satellite data to infer regional scale evapotranspiration. *IEEE. Transactions of Geosciences and Remote Sens*ing **28**, 940-958.

SADEGHI, M., BABAEIAN, E., TULLER, JONES, S. B., 2017: The optical trapezoid model: A novel approach to remote sensing of soil moisture applied to Sentinal-2 and Landsat-8 observations. *Remote Sensing of Environmen*t, **198**, 52-68.

SANDHOLT, I.; RASMUSSEN, K.; ANDERSEN, J.,2002. A simple interpretation of the surface temperature/vegetation index space for assessment of surface moisture status. *Remote Sensing of Environmen*t. **79,** 213-224.

SHEN, C., NIU, J., PHANIKUMAR, M. S., 2013. Evaluating controls on coupled hydrologic and vegetation dynamics in a humid continental climate watershed using a subsurface-land surface processes model. *Water Resources Research*, **49**(5), 2552-2572.

SILVA-FUZZO, CARLSON, T.N., KOURGIALAS, N., PETROPOULOS, G.P., 2019. A new technique for estimating soybean yield through remote sensing of soil moisture and evapotranspiration – A case study in Brazil. *Water MDPI*, submitted.

SILVA-FUZZO, D.F.; ROCHA, J.V., 2016. Simplified triangle method for estimating evaporative fraction over soybean crops. *Applied Remote Sensing*. **10**, 15pp.

SRIVASTAVA, P.K., D. HAN, A. YADUVANSHI, G.P. PETROPOULOS, S. K. SINGH, R. K. MALL & R. PRASAD, 2017. Reference Evapotranspiration Retrievals From a Mesoscale Model Based Weather Variables for Soil Moisture Deficit Estimation. *Sustainability*, **9**, 1971-88, doi:10.3390/su9111971

TANG, R.; LI, Z.; TANG, L., 2010. An application of the Ts-VI triangle method with enhanced edges determination for evapotranspiration estimation from MODIS data in arid and semi-arid regions: implementation and validation. *Remote Sensing of Environment*, **114**, 540-551.

TIAN, F., QIU, G., LÜ, Y., YANG, Y., XIONG, Y., 2014. Use of high-resolution thermal infrared remote sensing and "three-temperature model" for transpiration monitoring in arid inland river catchment. *Journal of Hydrology*, **515**, 307-315.

List of Figures:

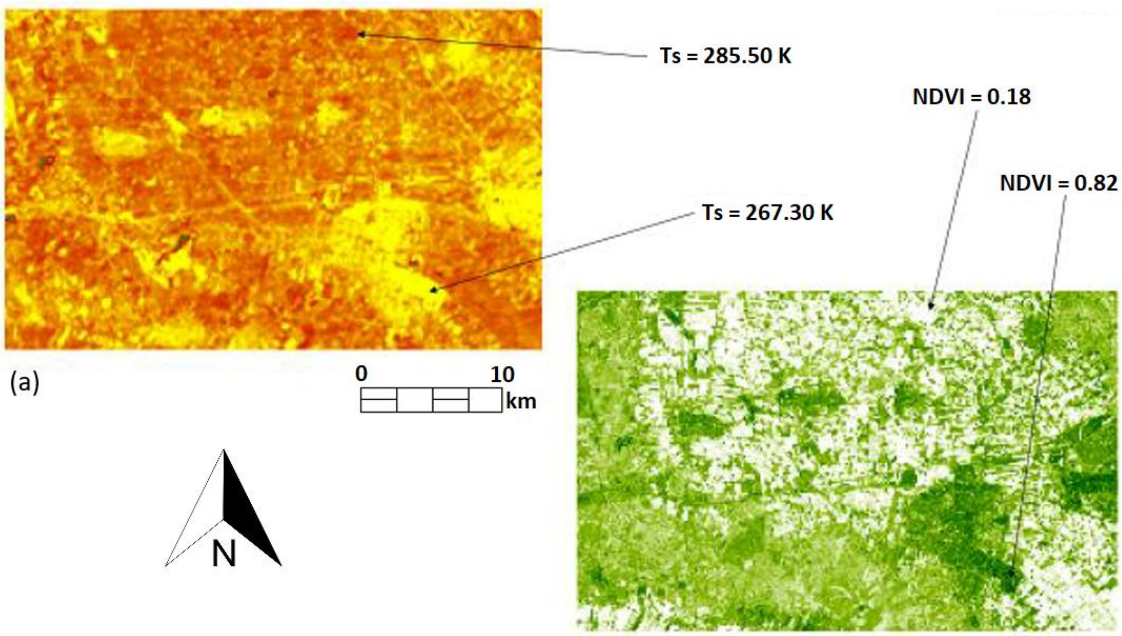

(b)

Figure 1: An example of a Surface Radiometric Temperature image (a) and NDVI image (b) derived from ASTER satellite Surface Kinetic Temperature Surface Reflectance products acquired for a region in The Netherlands on 30 March 2004. In (a), reds are the hottest and yellows the coolest pixels. Hottest and coolest pixels are labeled with arrows in degrees K. In the NDVI image (b) whites are the least vegetated and greens the most vegetated pixels with highest and lowest NDVI values labeled with arrows.

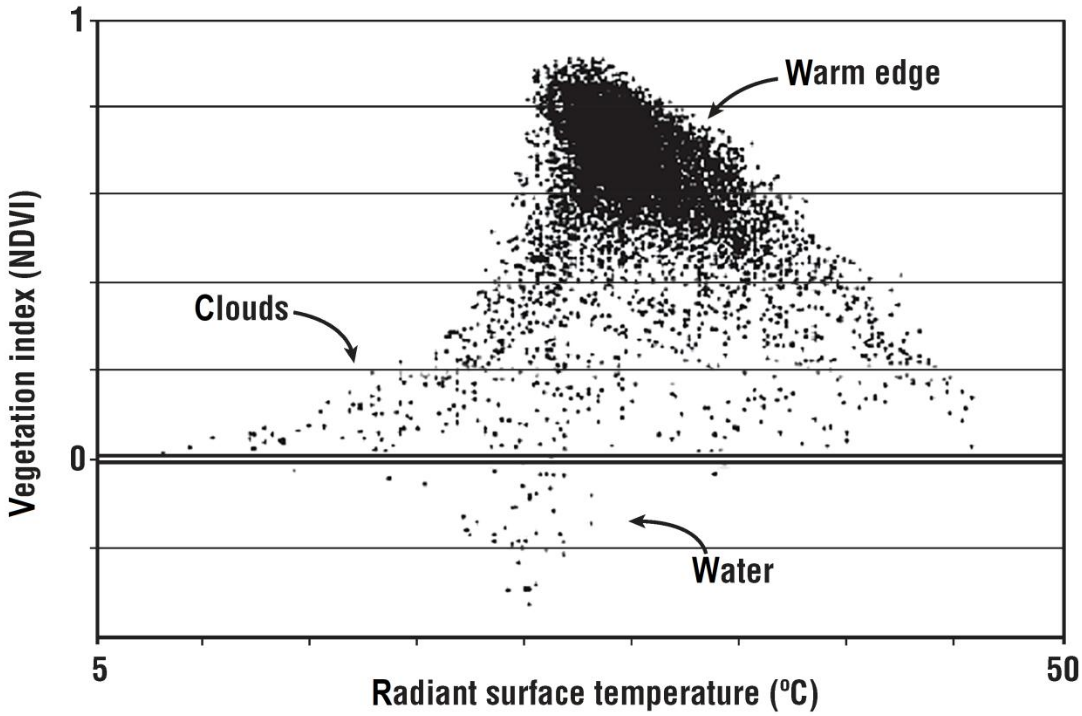

Figure 2: An example of a scatterplot created from the T_{ir} versus NDVI for an AVHRR image (referred to also in Arthur-Hartranft et al., 2003), originally from Owen et al., (1998). The horizontal axis is T_{ir} and the vertical axis is NDVI, showing $NDVI_o$ and $NDVI_s$ marked by horizontal lines.

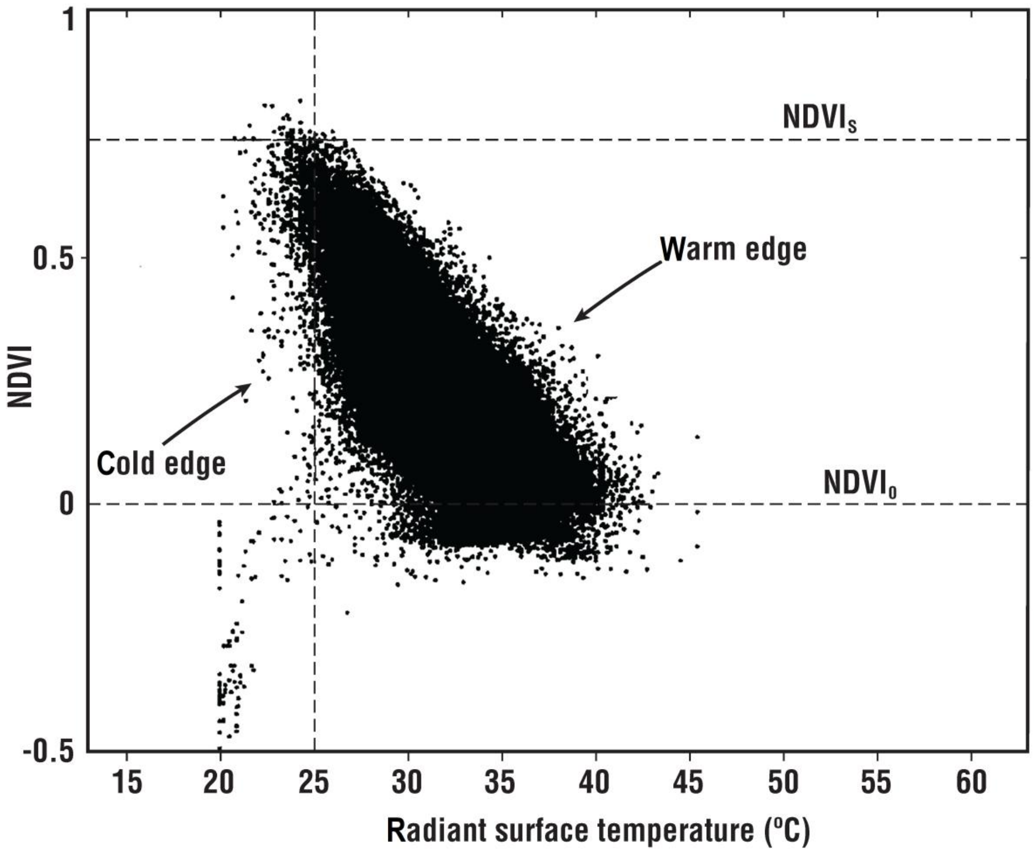

Figure 3: Triangle plotted as NDVI versus T_{ir} created from pixels measured by an aircraft radiometer (adopted from Gilles et al., 1997), showing the warm and cold edges.

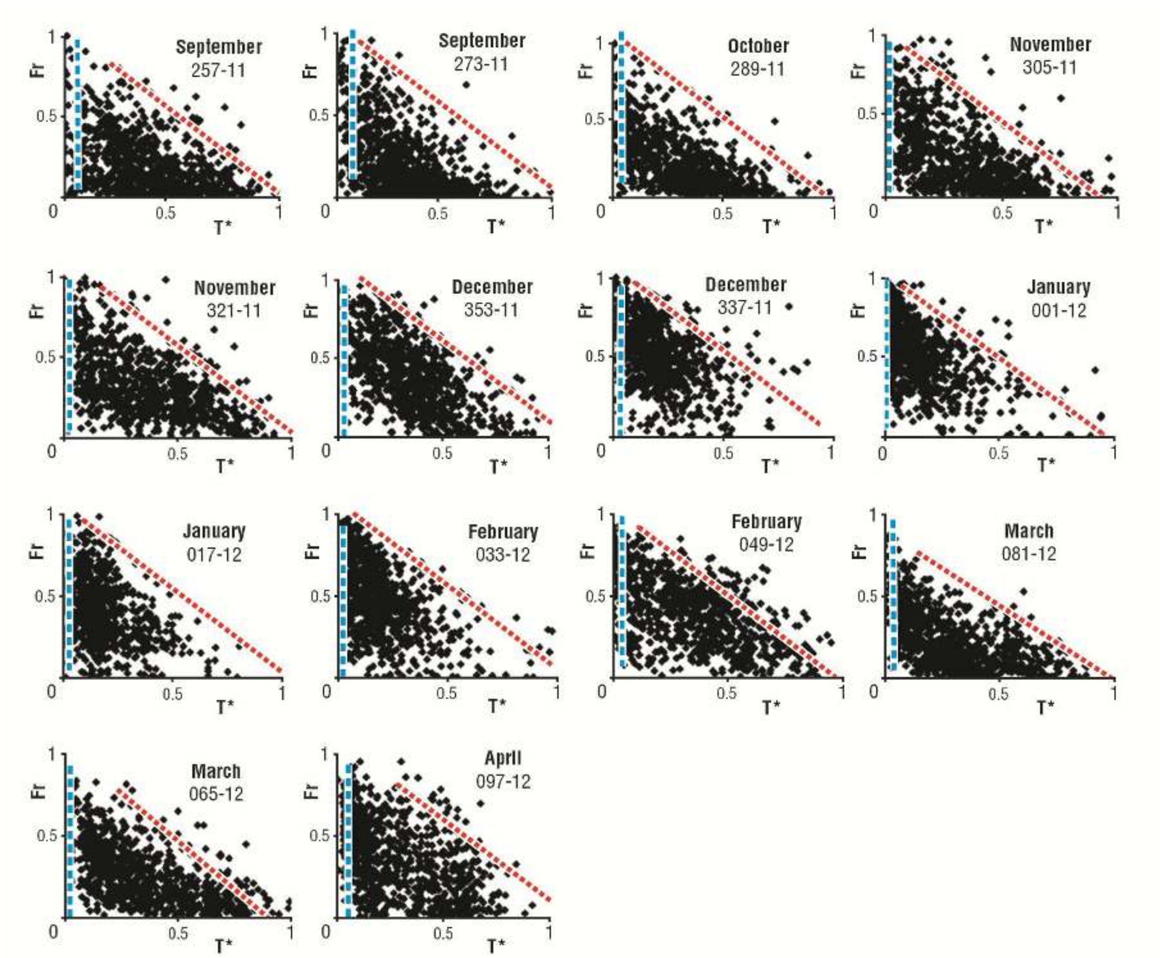

Figure 4: Examples of triangular shapes derived from images over soybean fields for Toledo County in Brazil, plotted as in the previous figures, with fractional vegetation (here called F_r) along the vertical and T^* along the horizontal. The sloping red line is the defined warm edge and the vertical blue line is the cold edge. The soil line corresponds to the lower (horizontal) axis (adapted from Silva-Fuzzo & Rocha, 2016)

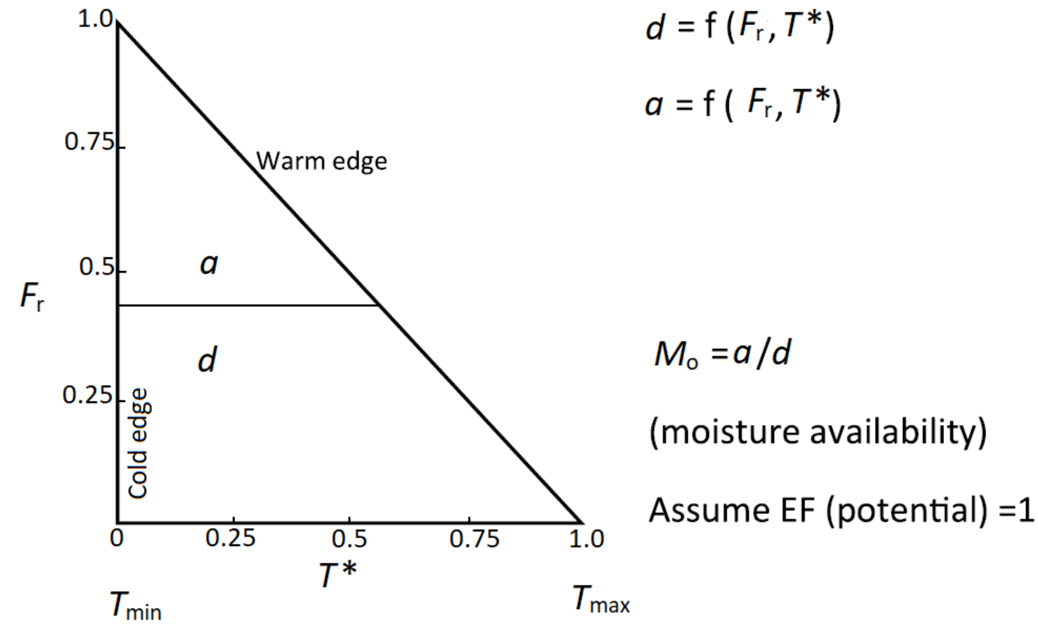

Figure 5: Conceptualization of the structure and solution of the triangle domain using the "simplified triangle" method based on Equations 5-8. The horizontal segment represents any slice across the triangle at constant Fr, where the letters a and d represent, respectively, a part of the segment and its entire length.

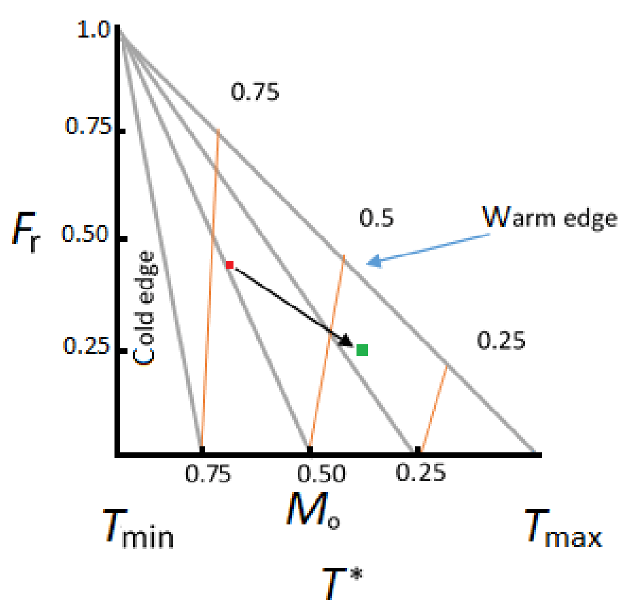

Figure 6: The 'universal triangle' (F_r versus T^*). Isopleths of EF (slanting lines toward the right, labelled accordingly along the warm edge) and M_o (slanting lines to the left, labelled along the horizontal for the solution of Equations (5)-(8). The arrow segment represents a surface pixel drying with time (from red

square to green square). T^* varies from zero at the lower left vertex to 1.0 at the lower right vertex.

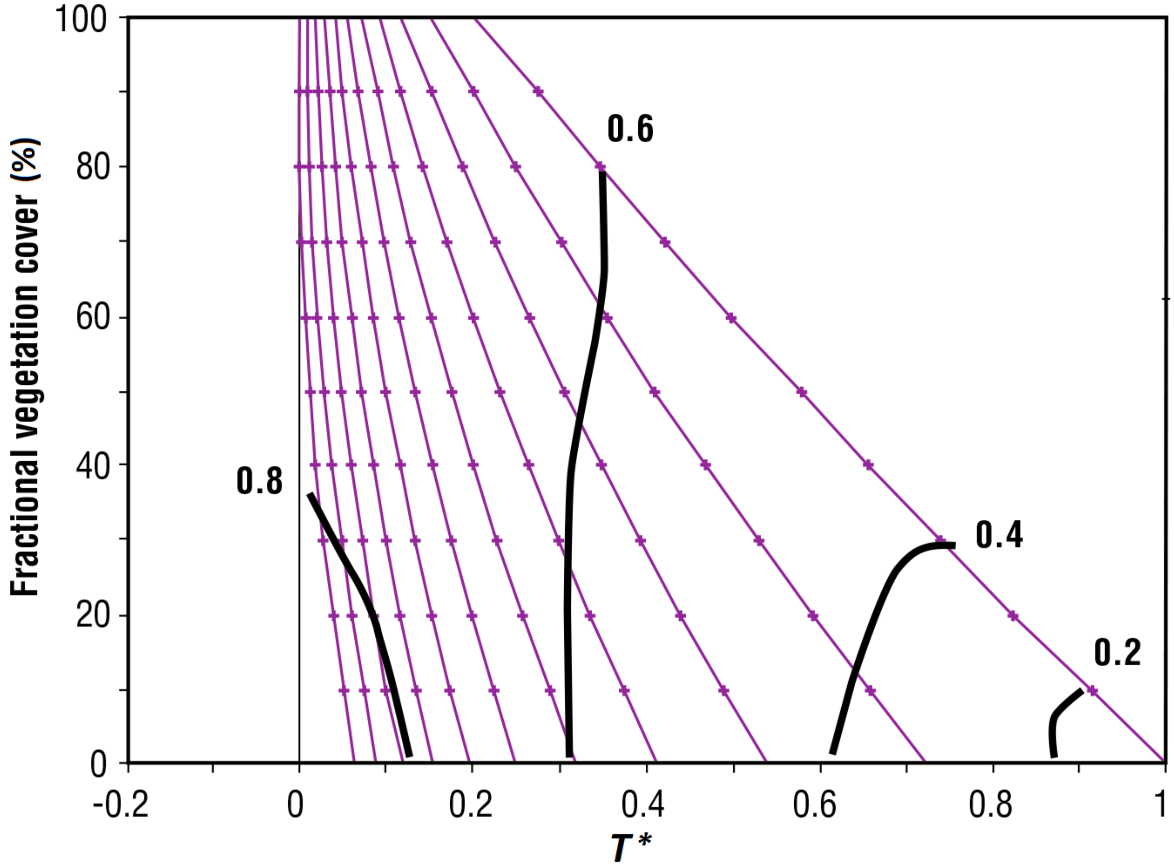

Figure 7: Numerical solution for isopleths of M_o (solid lines sloping upward to the left and labeled at 0.1 increments) and EF (solid black lines) versus F_r (percent) and T^* (horizontal axis) (adopted from Carlson & Sanchez-Azofeifa, 1998).